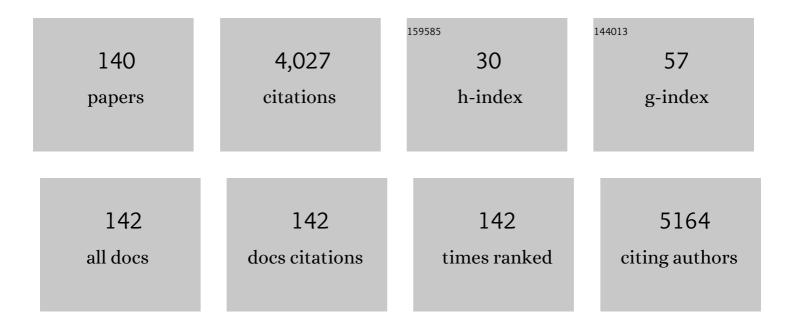
## Long Zhang

List of Publications by Year in descending order

Source: https://exaly.com/author-pdf/1426958/publications.pdf Version: 2024-02-01



#	Article	IF	CITATIONS
1	Direct Observation of Degenerate Two-Photon Absorption and Its Saturation in WS <sub>2</sub> and MoS <sub>2</sub> Monolayer and Few-Layer Films. ACS Nano, 2015, 9, 7142-7150.	14.6	322
2	Optical Limiting and Theoretical Modelling of Layered Transition Metal Dichalcogenide Nanosheets. Scientific Reports, 2015, 5, 14646.	3.3	236
3	Ultrafast Nonlinear Excitation Dynamics of Black Phosphorus Nanosheets from Visible to Mid-Infrared. ACS Nano, 2016, 10, 6923-6932.	14.6	231
4	Single-Mode Lasers Based on Cesium Lead Halide Perovskite Submicron Spheres. ACS Nano, 2017, 11, 10681-10688.	14.6	216
5	Hybridization-induced broadband terahertz wave absorption with graphene metasurfaces. Optics Express, 2018, 26, 11728.	3.4	188
6	Giant twoâ€photon absorption in monolayer MoS <sub>2</sub> . Laser and Photonics Reviews, 2015, 9, 427-434.	8.7	161
7	Covalent functionalization of reduced graphene oxide with porphyrin by means of diazonium chemistry for nonlinear optical performance. Scientific Reports, 2016, 6, 23325.	3.3	98
8	Short- and Medium-Range Order in Sodium Aluminophosphate Glasses:Â New Insights from High-Resolution Dipolar Solid-State NMR Spectroscopy. Journal of Physical Chemistry B, 2006, 110, 8946-8958.	2.6	93
9	Large-scale, low-cost, broadband and tunable perfect optical absorber based on phase-change material. Nanoscale, 2020, 12, 5374-5379.	5.6	92
10	Tunable effective nonlinear refractive index of graphene dispersions during the distortion of spatial self-phase modulation. Applied Physics Letters, 2014, 104, .	3.3	84
11	Bacterially synthesized tellurium nanostructures for broadband ultrafast nonlinear optical applications. Nature Communications, 2019, 10, 3985.	12.8	68
12	Nonlinear Optical Signatures of the Transition from Semiconductor to Semimetal in PtSe <sub>2</sub> . Laser and Photonics Reviews, 2019, 13, 1900052.	8.7	64
13	Medium-Range Order in Sol–Gel Prepared Al <sub>2</sub> O <sub>3</sub> –SiO <sub>2</sub> Glasses: New Results from Solid-State NMR. Journal of Physical Chemistry C, 2014, 118, 4906-4917.	3.1	61
14	MoS <sub>2</sub> /Carbon Nanotube Core–Shell Nanocomposites for Enhanced Nonlinear Optical Performance. Chemistry - A European Journal, 2017, 23, 3321-3327.	3.3	57
15	Single-crystalline tower-like ZnO microrod UV lasers. Journal of Materials Chemistry C, 2013, 1, 202-206.	5.5	55
16	Intense multiphoton upconversion of Yb <sup>3+</sup> –Tm <sup>3+</sup> doped β-NaYF <sub>4</sub> individual nanocrystals by saturation excitation. Journal of Materials Chemistry C, 2015, 3, 364-369.	5.5	55
17	Cooperative excitonic quantum ensemble in perovskite-assembly superlattice microcavities. Nature Communications, 2020, 11, 329.	12.8	51
18	Ultrahigh Quality Upconverted Singleâ€Mode Lasing in Cesium Lead Bromide Spherical Microcavity. Advanced Optical Materials, 2018, 6, 1800391.	7.3	47

#	Article	IF	CITATIONS
19	Slow and fast absorption saturation of black phosphorus: experiment and modelling. Nanoscale, 2016, 8, 17374-17382.	5.6	46
20	Tunable and transparent broadband metamaterial absorber with water-based substrate for optical window applications. Nanoscale, 2021, 13, 7831-7837.	5.6	44
21	The effect of La2O3 in Tm3+-doped germanate-tellurite glasses for ~2â€Î¼m emission. Scientific Reports, 2014, 4, 5256.	3.3	43
22	High-performance broadband electromagnetic interference shielding optical window based on a metamaterial absorber. Optics Express, 2020, 28, 26836.	3.4	41
23	Two-photon absorption and emission in CsPb(Br/I) <sub>3</sub> cesium lead halide perovskite quantum dots. CrystEngComm, 2016, 18, 7945-7949.	2.6	40
24	Direct synthesis of large-scale hierarchical MoS <sub>2</sub> films nanostructured with orthogonally oriented vertically and horizontally aligned layers. Nanoscale, 2016, 8, 431-439.	5.6	39
25	Graphene and Carbon Nanotube Polymer Composites for Laser Protection. Journal of Inorganic and Organometallic Polymers and Materials, 2011, 21, 736-746.	3.7	37
26	Single-mode lasing and 3D confinement from perovskite micro-cubic cavity. Journal of Materials Chemistry C, 2018, 6, 11740-11748.	5.5	37
27	Surface-State Assisted Carrier Recombination and Optical Nonlinearities in Bulk to 2D Nonlayered PtS. ACS Nano, 2019, 13, 13390-13402.	14.6	37
28	Intense photoluminescence at 27 μm in transparent Er^3+:CaF_2-fluorophosphate glass microcomposite. Optics Letters, 2011, 36, 4347.	3.3	35
29	High-Temperature Upconverted Single-Mode Lasing in 3D Fully Inorganic Perovskite Microcubic Cavity. ACS Photonics, 2019, 6, 793-801.	6.6	35
30	TiO <sub>2</sub> –multi-walled carbon nanotube nanocomposites: hydrothermal synthesis and temporally-dependent optical properties. RSC Advances, 2016, 6, 20120-20127.	3.6	32
31	Multi-walled carbon nanotubes covalently functionalized by axially coordinated metal-porphyrins: Facile syntheses and temporally dependent optical performance. Nano Research, 2016, 9, 458-472.	10.4	31
32	Switchable ultra-broadband terahertz wave absorption with VO2-based metasurface. Scientific Reports, 2022, 12, 2501.	3.3	30
33	Structural Role of Fluoride in Aluminophosphate Solâ^Gel Glasses:  High-Resolution Double-Resonance NMR Studies. Journal of Physical Chemistry B, 2007, 111, 10402-10412.	2.6	29
34	Fabrication of transparent yttria ceramics by alcoholic slip-casting. Ceramics International, 2017, 43, 8839-8844.	4.8	29
35	Investigation of optical, mechanical, and thermal properties of ZrO2-doped Y2O3 transparent ceramics fabricated by HIP. Ceramics International, 2018, 44, 1362-1369.	4.8	29
36	Structural Studies of NaPO <sub>3</sub> –AlF <sub>3</sub> Glasses by High-Resolution Double-Resonance Nuclear Magnetic Resonance Spectroscopy. Journal of Physical Chemistry C, 2018, 122, 21579-21588.	3.1	29

#	Article	IF	CITATIONS
37	Energy transfer and wavelength tunable lasing of single perovskite alloy nanowire. Nano Energy, 2020, 71, 104641.	16.0	29
38	Double-layer metal mesh etched by femtosecond laser for high-performance electromagnetic interference shielding window. RSC Advances, 2019, 9, 22282-22287.	3.6	28
39	Quantum Dot Selfâ€Assembly Enables Lowâ€Threshold Lasing. Advanced Science, 2021, 8, e2101125.	11.2	28
40	Fabrication of large-volume microfluidic chamber embedded in glass using three-dimensional femtosecond laser micromachining. Microfluidics and Nanofluidics, 2011, 11, 111-117.	2.2	26
41	Optical absorption and mechanism of vacuum-sintered ZrO2-doped Y2O3 ceramics. Journal of the European Ceramic Society, 2016, 36, 4181-4184.	5.7	26
42	Grayscale image recording on Ge2Sb2Te5 thin films through laser-induced structural evolution. Scientific Reports, 2017, 7, 42712.	3.3	25
43	Influence of moisture absorption on the synthesis and properties of Y2O3–MgO nanocomposites. Ceramics International, 2017, 43, 40-44.	4.8	25
44	Ultrastable low-cost colloidal quantum dot microlasers of operative temperature up to 450 K. Light: Science and Applications, 2021, 10, 60.	16.6	25
45	Broad-band lead halide perovskite quantum dot single-mode lasers. Journal of Materials Chemistry C, 2020, 8, 13642-13647.	5.5	24
46	Fabrication of fine-grained undoped Y2O3 transparent ceramic using nitrate pyrogenation synthesized nanopowders. Ceramics International, 2019, 45, 5339-5345.	4.8	23
47	Optical identification of layered MoS2via the characteristic matrix method. Nanoscale, 2016, 8, 1210-1215.	5.6	22
48	Effects of deformation rate on properties of Nd,Y-codoped CaF 2 transparent ceramics. Journal of the European Ceramic Society, 2018, 38, 2404-2409.	5.7	22
49	Linearly polarized lasing based on coupled perovskite microspheres. Nanoscale, 2020, 12, 5805-5811.	5.6	22
50	Structural Studies of Fluoroborate Laser Glasses by Solid State NMR and EPR Spectroscopies. Journal of Physical Chemistry C, 2017, 121, 741-752.	3.1	21
51	Functionalization of reduced graphene oxide with axially-coordinated metal-porphyrins: facile syntheses and temporally-dependent nonlinear optical properties. Inorganic Chemistry Frontiers, 2016, 3, 296-305.	6.0	20
52	Transparent Nd-doped Ca1â^'xYxF2+x ceramics prepared by the ceramization of single crystals. Materials and Design, 2017, 113, 326-330.	7.0	20
53	Facet-dependent nonlinear optical properties of bismuth oxychloride single-crystal nanosheets. Journal of Materials Chemistry C, 2018, 6, 8709-8716.	5.5	20
54	Geometry Dependent Evolution of the Resonant Mode in ZnO Elongated Hexagonal Microcavity. Scientific Reports, 2016, 6, 19273.	3.3	19

#	Article	IF	CITATIONS
55	Surfaceâ€Energyâ€Driven Growth of ZnO Hexagonal Microtube Optical Resonators. Advanced Optical Materials, 2016, 4, 126-134.	7.3	19
56	Colloidal quantum-dot-based silica gel glass: two-photon absorption, emission, and quenching mechanism. Nanoscale, 2016, 8, 16440-16448.	5.6	19
57	Generic synthesis and versatile applications of molecularly organic–inorganic hybrid mesoporous organosilica nanoparticles with asymmetric Janus topologies and structures. Nano Research, 2017, 10, 3790-3810.	10.4	19
58	CdTe/CdS Quantum Dots: Effective Saturable Absorber for Visible Lasers. IEEE Journal of Selected Topics in Quantum Electronics, 2017, 23, 1-7.	2.9	19
59	Mid-infrared laser emission from Cr:ZnS channel waveguide fabricated by femtosecond laser helical writing. Scientific Reports, 2016, 5, 18365.	3.3	18
60	Er 3+ -doped oxyfluorogallate glass for 2.7 Âμm solid-state lasers. Journal of Luminescence, 2016, 172, 331-334.	3.1	18
61	Next generation mid-infrared fiber: fluoroindate glass fiber. Optical Materials Express, 2022, 12, 1683.	3.0	18
62	Sol–gel preparation of mesoporous Al2O3–SiO2 glasses: structural evolution monitored by solid state NMR. Journal of Sol-Gel Science and Technology, 2014, 70, 482-490.	2.4	17
63	Low-temperature-flux syntheses of ultraviolet-transparent borophosphates Na <sub>4</sub> MB <sub>2</sub> P <sub>3</sub> O <sub>13</sub> (M = Rb, Cs) exhibiting a second-harmonic generation response. Dalton Transactions, 2017, 46, 12605-12611.	3.3	17
64	Transparent ultra-wideband double-resonance-layer metamaterial absorber designed by a semiempirical optimization method. Optics Express, 2021, 29, 18446.	3.4	17
65	Auger-type process in ultrathin ReS <sub>2</sub> . Optical Materials Express, 2020, 10, 1092.	3.0	17
66	Nanolayered VO <sub>2</sub> -Based Switchable Terahertz Metasurfaces as Near-Perfect Absorbers and Antireflection Coatings. ACS Applied Nano Materials, 2022, 5, 5569-5577.	5.0	17
67	Sol-gel synthesis of sodium-modified AlPO4–SiO2 glasses and structural characterization by solid state NMR. Journal of Materials Chemistry, 2009, 19, 1151.	6.7	15
68	Tailoring the Luminescence of Europium Ions in Mesoporous AlPO <sub>4</sub> Monolithic Glass. Journal of Physical Chemistry C, 2013, 117, 21916-21922.	3.1	15
69	Europium doped transparent glass ceramics containing CaF <sub>2</sub> micron-sized crystals: structural and optical characterization. RSC Advances, 2016, 6, 55366-55373.	3.6	15
70	Influence of synthesis conditions on the properties of Y2O3–MgO nanopowders and sintered nanocomposites. Journal of the European Ceramic Society, 2017, 37, 4095-4101.	5.7	15
71	A novel synthesis and excellent photodegradation of flower-like ZnO hierarchical microspheres. CrystEngComm, 2013, 15, 10272.	2.6	14
72	Optical and thermal properties of TiO <sub>2</sub> â€doped Y <sub>2</sub> O <sub>3</sub> transparent ceramics synthesized by hot isostatic pressing. Journal of the American Ceramic Society, 2019, 102, 2021-2028.	3.8	14

#	Article	IF	CITATIONS
73	Large-size oxyfluoride glasses used for vis–IR-transmitting windows. Journal of Non-Crystalline Solids, 2009, 355, 2006-2009.	3.1	13
74	Precipitation and Growth Mechanism of Diverse Sr <sub>5</sub> ( <scp>PO</scp> <sub>4</sub> ) <sub>3</sub> F Particles. Journal of the American Ceramic Society, 2016, 99, 1498-1503.	3.8	13
75	Perfectly transparent pore-free Nd3+-doped Sr9GdF21 polycrystalline ceramics elaborated from single-crystal ceramization. Journal of the European Ceramic Society, 2017, 37, 4912-4918.	5.7	13
76	Efficient Energy and Electron Transfer between Donor and Acceptor Chromophores in Aluminophosphate Hybrid Materials. Journal of the Chinese Chemical Society, 2010, 57, 539-546.	1.4	12
77	Rapid identification of H5 avian influenza virus in chicken throat swab specimens using microfluidic real-time RT-PCR. Analytical Methods, 2014, 6, 2628.	2.7	12
78	An Allâ€Inorganic Perovskiteâ€Phase Rubidium Lead Bromide Nanolaser. Angewandte Chemie - International Edition, 2019, 58, 16134-16140.	13.8	12
79	Femtosecond laser-induced damage characteristics of mid-infrared oxyfluorogallate glass. Optics and Laser Technology, 2019, 109, 659-665.	4.6	12
80	Polariton–Polariton Interactions Revealed in a One-dimensional Whispering Gallery Microcavity. Nano Letters, 2020, 20, 1552-1560.	9.1	12
81	Thermodynamic-effect-induced growth, optical modulation and UV lasing of hierarchical ZnO Fabry–Pérot resonators. Journal of Materials Chemistry, 2012, 22, 3069.	6.7	11
82	Optical modulation of ZnO microwire optical resonators with a parallelogram cross-section. Nanoscale, 2013, 5, 4123.	5.6	11
83	Optical modulation in microsized optical resonators with irregular hexagonal cross-section. Journal of Materials Chemistry C, 2014, 2, 8976-8982.	5.5	11
84	Preparation and Optical Properties of Infrared Transparent 3Y-TZP Ceramics. Materials, 2017, 10, 390.	2.9	11
85	Near-field imaging of the multi-resonant mode induced broadband tunable metamaterial absorber. RSC Advances, 2020, 10, 5146-5151.	3.6	11
86	Nonlinear optical propagation in a tandem structure comprising nonlinear absorption and scattering materials. Applied Physics Letters, 2014, 104, 021110.	3.3	10
87	Effects of annealing on Cr-sensitized Nd:LuAG laser ceramics. Optical Materials Express, 2015, 5, 2209.	3.0	10
88	Recrystallization of Er <sup>3+</sup> :CaF <sub>2</sub> in Transparent Fluorophosphate Glassâ€Ceramics with the Coâ€Firing Method. Journal of the American Ceramic Society, 2016, 99, 2971-2976.	3.8	10
89	High transparency Cr,Nd:LuAG ceramics prepared with MgO additive. Journal of the European Ceramic Society, 2017, 37, 2459-2463.	5.7	10
90	Temperature dependent thermal conductivity and transition mechanism in amorphous and crystalline Sb2Te3 thin films. Scientific Reports, 2017, 7, 13747.	3.3	10

#	Article	IF	CITATIONS
91	Ultrafast Saturable Absorption of Core/Shell Colloidal Quantum Dots. Particle and Particle Systems Characterization, 2017, 34, 1600193.	2.3	10
92	YAG/Nd:LuAG composite laser materials prepared by the ceramization of YAG single crystals. Journal of the European Ceramic Society, 2018, 38, 1966-1971.	5.7	10
93	Phase-separation engineering in fluorozirconate glass for designing and fabricating of transparent perfluorinate glass ceramic. Journal of the European Ceramic Society, 2020, 40, 3244-3248.	5.7	10
94	Allâ€Photonic Miniature Perovskite Encoder with a Terahertz Bandwidth. Laser and Photonics Reviews, 2020, 14, 1900398.	8.7	10
95	Preparation of LuAG Powders with Single Phase and Good Dispersion for Transparent Ceramics Using Co-Precipitation Method. Materials, 2015, 8, 5363-5375.	2.9	9
96	Highly-oriented (104) polycrystalline α-Al2O3 transparent ceramics prepared by a templated grain growth method. Journal of the European Ceramic Society, 2019, 39, 1721-1724.	5.7	9
97	Free‧tanding, Singleâ€Crystalline Parallelogram Sb Shallowâ€Doped ZnO Waveâ€Guided Optical Resonators. Advanced Optical Materials, 2014, 2, 1090-1097.	7.3	8
98	Origin of arbitrary patterns by direct laser writing in a telluride thin film. RSC Advances, 2016, 6, 45748-45752.	3.6	8
99	Sol–gel derived mesoporous GaAlPO <sub>4</sub> glass for heavy metal ion sequestration. RSC Advances, 2016, 6, 99149-99157.	3.6	8
100	Spatial ions distribution of the bonding interface in <scp>YAG</scp> /Nd:Lu <scp>AG</scp> composite laser ceramic. Journal of the American Ceramic Society, 2017, 100, 5030-5037.	3.8	8
101	On fast LuAG:Ce scintillation ceramics with Ca <sup>2+</sup> coâ€dopants. Journal of the American Ceramic Society, 2021, 104, 966-973.	3.8	8
102	Joint latent low-rank and non-negative induced sparse representation for face recognition. Applied Intelligence, 2021, 51, 8349.	5.3	8
103	Demonstration of Thermally Tunable Multi-Band and Ultra-Broadband Metamaterial Absorbers Maintaining High Efficiency during Tuning Process. Materials, 2021, 14, 5708.	2.9	8
104	Femtosecond-scale all-optical switching in oxyfluorogallate glass induced by nonlinear multiphoton absorption. RSC Advances, 2021, 11, 32446-32453.	3.6	8
105	Ultrafast Optical Properties of Cavityâ€Enhanced Superfluorescence. Advanced Optical Materials, 2022, 10, .	7.3	8
106	Doping limit and site occupation of Yb <sup>3+</sup> in strontium fluoroapatite. RSC Advances, 2016, 6, 88868-88873.	3.6	7
107	Manipulation and simulations of thermal field profiles in laser heat-mode lithography. Journal of Applied Physics, 2017, 122, .	2.5	7
108	Heatâ€driven Tailored for Eliminating Nd 3+ Reâ€clusters in Nd 3+ ,Gd 3+ â€codoped SrF 2 Laser Ceramic. Journal of the American Ceramic Society, 2020, 103, 2562-2568.	3.8	7

#	Article	IF	CITATIONS
109	Fabrication of infrared-transparent Y2O3–MgO composites using nanopowders synthesized via thermal decomposition. Ceramics International, 2021, 47, 13007-13014.	4.8	7
110	Preparation and study of the mechanical and optical properties of infrared transparent Y <sub>2</sub> O <sub>3</sub> –MgO composite ceramics. Journal of the American Ceramic Society, 2021, 104, 6335-6344.	3.8	7
111	Relaxation Oscillations of an Exciton–Polariton Condensate Driven by Parametric Scattering. Nano Letters, 2022, 22, 3026-3032.	9.1	7
112	Er3+ concentration-dependent microstructural and upconversion luminescence process of transparent perfluoride composite glass. Journal of the European Ceramic Society, 2022, 42, 4335-4342.	5.7	7
113	Influence of dopant concentration on the transparent and thermal properties of Nd 2 O 3 -doped alumina translucent ceramics. Journal of Rare Earths, 2017, 35, 883-886.	4.8	6
114	An Allâ€Inorganic Perovskiteâ€Phase Rubidium Lead Bromide Nanolaser. Angewandte Chemie, 2019, 131, 16280-16286.	2.0	6
115	Perfluoride glass ceramic transmitting from UV to far-IR tailored by one step. Optics Letters, 2019, 44, 4857.	3.3	6
116	Samarium and manganese incorporation to improve color rendering of LuAG:Ce <sup>3+</sup> phosphor ceramics for laser-driven lighting: a Color-tunable and energy transfer study. Journal of Materials Chemistry C, 2021, 9, 16468-16476.	5.5	6
117	Surface Structure and Electronic Properties of Lu3Al5O12. Crystals, 2021, 11, 1433.	2.2	6
118	Homogeneity of Inorganic Glasses: Quantification and Ranking. International Journal of Applied Glass Science, 2011, 2, 137-143.	2.0	5
119	Tunable and white light emitting AlPO4 mesoporous glass by design of inorganic/organic luminescent species. APL Materials, 2015, 3, 046101.	5.1	5
120	Er <sup>3+</sup> â€doped CaF <sub>2</sub> polycrystalline ceramic with perfect transparency for midâ€infrared laser. Journal of the American Ceramic Society, 2020, 103, 5808-5812.	3.8	5
121	Phase-Type Fresnel Zone Plate with Multi-Wavelength Imaging Embedded in Fluoroaluminate Glass Fabricated via Ultraviolet Femtosecond Laser Lithography. Micromachines, 2021, 12, 1362.	2.9	5
122	Enhanced near-infrared transmission of ZnO-doped Y2O3–MgO nanocomposites with reduced light scattering due to decreased refractive index difference. Journal of the European Ceramic Society, 2022, 42, 4616-4622.	5.7	5
123	Re-clustering of neodymium ions in neodymium, buffer ion-codoped alkaline-earth fluoride transparent ceramics. CrystEngComm, 2017, 19, 4480-4484.	2.6	4
124	Glass-forming ability control of Er3+-Doped lithium-modified fluorozirconate glass. Ceramics International, 2019, 45, 24115-24120.	4.8	4
125	Non-linear changes of performances caused by introduction of chloride ions into Er3+-doped fluorozirconate glass. Ceramics International, 2019, 45, 4431-4436.	4.8	4
126	Time-resolved online analysis of the gas- and particulate-phase of cigarette smoke generated by a heated tobacco product using vacuum ultraviolet photoionization mass spectrometry. Talanta, 2022, 238, 123062.	5.5	4

#	Article	IF	CITATIONS
127	Structural Studies of Bi <sub>2</sub> O <sub>3</sub> –NaPO <sub>3</sub> Glasses by Solid State Nuclear Magnetic Resonance and X-ray Photoelectron Spectroscopy. Journal of Physical Chemistry C, 2017, 121, 10087-10094.	3.1	3
128	Facile synthesis and optical properties of colloidal quantum dots/ZnO composite optical resonators. RSC Advances, 2018, 8, 1778-1783.	3.6	3
129	Broadening emission band of Yb:LuScO 3 transparent ceramics for ultrashort pulse laser. Journal of the American Ceramic Society, 2021, 104, 6064-6073.	3.8	3
130	Stable Multiâ€Wavelength Lasing in Single Perovskite Quantum Dot Superlattice. Advanced Optical Materials, 0, , 2200494.	7.3	3
131	CLASSIFICATION OF SKIN AUTOFLUORESCENCE SPECTRUM USING SUPPORT VECTOR MACHINE IN TYPE 2 DIABETES SCREENING. Journal of Innovative Optical Health Sciences, 2013, 06, 1350036.	1.0	2
132	Performance and structure evolution of fluoindinate glass at high temperatures. Journal of the American Ceramic Society, 0, , .	3.8	2
133	Low thermal expansion ZBLANâ€based glass ceramics containing CaZrF <sub>6</sub> crystals. Journal of the American Ceramic Society, 2022, 105, 3959-3966.	3.8	2
134	Luminescence and structural evolution in ultraâ€low melting quaternary tin fluorophosphate glasses (NaFâ€5nF <sub>2</sub> â€5nOâ€P <sub>2</sub> O <sub>5</sub> ). Journal of the American Ceramic Society, 2022, 105, 2595-2604.	3.8	2
135	Granulation of Y <sub>2</sub> O <sub>3</sub> powders by a vibration method for the preparation of transparent ceramics. RSC Advances, 2016, 6, 105755-105760.	3.6	1
136	Defects & Luminescence of Lu <sub>3</sub> Al <sub>5</sub> O <sub>12</sub> Phosphor Doped with Na Ion. Chemistry Letters, 2021, 50, 1359-1362.	1.3	1
137	Solventâ€Mediated Structural Evolution in Colloidal Lead Halide Perovskite Nanocrystals Selfâ€Assembly. Advanced Materials Interfaces, 2022, 9, .	3.7	1
138	CHEMICAL MECHANICAL POLISHING AND ITS MECHANISM ON YTTERBIUM-DOPED MIXED SESQUIOXIDES (Yb:LuScO <sub>3</sub> ). Surface Review and Letters, 2021, 28, 2050036.	1.1	0
139	A novel approach and segregation behavior of heavily doped Nd:YAG/YAG composite structure by solid-state crystal growth. Optical Materials, 2022, 128, 112455.	3.6	0
140	Solventâ€Mediated Structural Evolution in Colloidal Lead Halide Perovskite Nanocrystals Selfâ€Assembly (Adv. Mater. Interfaces 19/2022). Advanced Materials Interfaces, 2022, 9, .	3.7	0